Phase reduction beyond the first order: The case of the mean-field complex Ginzburg-Landau equation

Iván León and Diego Pazó
Instituto de Física de Cantabria (IFCA), CSIC-Universidad de Cantabria, 39005 Santander, Spain

(Received 17 April 2019; published 19 July 2019)

Phase reduction is a powerful technique that makes possible to describe the dynamics of a weakly perturbed limit-cycle oscillator in terms of its phase. For ensembles of oscillators, a classical example of phase reduction is the derivation of the Kuramoto model from the mean-field complex Ginzburg-Landau equation (MF-CGLE). Still, the Kuramoto model is a first-order phase approximation that displays either full synchronization or incoherence, but none of the nontrivial dynamics of the MF-CGLE. This fact calls for an expansion beyond the first order in the coupling constant. We develop an isochron-based scheme to obtain the second-order phase approximation, which reproduces the weak-coupling dynamics of the MF-CGLE. The practicality of our method is evidenced by extending the calculation up to third order. Each new term of the power-series expansion contributes with additional higher-order multibody (i.e., nonpairwise) interactions. This points to intricate multibody phase interactions as the source of pure collective chaos in the MF-CGLE at moderate coupling.

DOI: 10.1103/PhysRevE.100.012211

I. INTRODUCTION

Networks of nonlinear elements with oscillatory behavior ("oscillators") are found in a variety of disciplines, such as neuroscience or engineering [1–4]. It is an empirical fact that some phenomena arising in these systems can be understood in terms of interacting phase oscillators. This framework has proven to be useful modeling and engineering experimental setups composed of many rhythmic elements, operating in a wide range of spatiotemporal scales, and interacting through very different physical processes. We may cite small motors—cell phone vibrators—interacting through an elastic plate [5], networks of (electro)chemical oscillators [6,7], arrays of Josephson junctions [8,9] and globally coupled electrical self-oscillators [10,11], or nanoelectromechanical oscillators in a ring [12].

Applying a phase-reduction method [1,13–15] is the rigorous way of describing a weakly perturbed oscillator solely in terms of its phase (the other degrees of freedom become enslaved). However, obtaining analytically the approximate "phase-only model" for a specific system is not an easy task. Moreover, phase reduction becomes inaccurate unless the disturbances are not sufficiently weak. While according to common wisdom phase reduction of oscillator ensembles yields pairwise interacting phase oscillators [13], multibody (i.e., nonpairwise) interactions may also be relevant in some contexts. Apart from the idea of invoking hypothetical three-body interacting limit-cycle oscillators [16], multibody phase interactions naturally arise if the coupling is nonlinear [17]; see also [18]. Instead, for linear pairwise coupling, three-body interactions are a distinctive element of second-order phase approximations, as recently highlighted in [12]. Recognizing the ubiquity of multibody interactions may also be important for reconstructing phase interactions from data [19].

Much of our knowledge on nonlinear dynamics relies on minimal models that capture the essential mechanisms behind complex phenomena. For oscillatory dynamics, the conventional test bed is the normal form of the Hopf bifurcation above criticality: the so-called Stuart-Landau oscillator. Concerning geometry, global coupling is a fruitful simplifying assumption [1,13,20]. These two ingredients are combined in a standard model of collective dynamics: the fully connected network of Stuart-Landau oscillators, or the mean-field version of the complex Ginzburg-Landau equation (MF-CGLE) [21–36]. This system is particularly interesting for chaos theory since it exhibits both microscopic (extensive) and macroscopic (collective) chaos, either combined or independently, depending on parameters [21–24,26,30,33,36]. Phase reduction of the MF-CGLE yields the Kuramoto-Sakaguchi model [13,22,37], a first-order approximation that behaves in a pathological way (unless heterogeneities are present): it only displays full synchrony or incoherence. Therefore, pure collective chaos and other phase dynamics of the MF-CGLE remain to be analytically described in terms of a phase model. Such a phase reduction should provide additional insights into the nature of collective chaos (playing an analogous role to the Kuramoto-Sivashinsky equation of phase turbulence).

The aim of this paper is twofold: we introduce a phase-reduction method, and we investigate the phase model obtained from the MF-CGLE. The paper is organized as follows. In Sec. II, we reexamine the phase dynamics of the MF-CGLE and the connection with its first-order phase reduction (the Kuramoto model). In Sec. III, we present our systematic phase-reduction procedure, based on the direct use of isochrons, which delivers a well-controlled power expansion in the coupling strength parameter. Section IV is devoted to investigating the weak-coupling limit of the MF-CGLE by means of the second-order phase reduction, which unfolds the

degeneracies of the Kuramoto model; we address the cases of a large ensemble of oscillators, as well as a small one of four oscillators. Section V presents the third-order contribution to the phase reduction of the MF-CGLE. Finally, in Sec. VI we discuss the implications of our work and some outlooks.

II. MEAN-FIELD COMPLEX GINZBURG-LANDAU EQUATION

The MF-CGLE consists of N diffusively coupled Stuart-Landau oscillators governed by N coupled (complex-valued) ordinary differential equations:

$$\dot{A}_j = A_j - (1 + ic_2)|A_j|^2 A_j + \epsilon(1 + ic_1)(\bar{A} - A_j). \quad (1)$$

Here, $A_j = r_j e^{i\varphi_j}$ is a complex variable (index j runs from 1 to N), and the mean field is $\bar{A} = N^{-1}\sum_{k=1}^{N} A_k$. Apart from the population size N, there are three free parameters in Eq. (1): ϵ, c_1, and c_2. Parameter ϵ, controlling the coupling strength, is positive in order to preserve the analogy with the (spatially extended) Ginzburg-Landau equation. Parameter c_1 introduces a cross-coupling between real and imaginary parts of the A_j's. This nondissipative coupling, so-called "reactive" [4], generically appears from center manifold reduction [13]. Finally, "nonisochronicity" (or "shear") parameter c_2 in Eq. (1) determines the dependence of the angular velocity of one oscillator on its radial coordinate.

There are two important symmetries in system (1): invariance under a global phase shift $A_j \to A_j e^{i\phi}$, and full permutation symmetry stemming from the mean-field coupling.

A. Phenomenology

For many parameter values, the global attractor of Eq. (1) is either full synchronization (FS) $A_j = \bar{A} = e^{-ic_2 t}$ or one incoherent state with vanishing mean field $\bar{A} = 0$. In the latter case, the oscillators rotate freely, $A_j = \sqrt{1-\epsilon}\exp\{i[-c_2 + \epsilon(c_2 - c_1)]t + \phi_j\}$. Among all the states compatible with $\bar{A} = 0$, the most prominent one is the uniform incoherent state (UIS) in which the ϕ_j are uniformly distributed in the thermodynamic limit (for a finite ensemble, the ϕ_j are evenly spaced, deserving the name of splay state or ponies on a merry-go-round state). A continuum of nonuniform incoherent states (NUISs) coexists with UIS, but usually arbitrarily weak noise spreads the phases and UIS is eventually attained. Nonetheless, for certain parameters values, such as those in Fig. 1(a), the UIS is unstable and one NUIS sets in spontaneously [21,25].

In addition to FS, UIS, and NUIS, system (1) exhibits a rich repertoire of collective states including clustering [22,27–29,33,35], diffusion-induced inhomogeneity (or chimera) [28,29,32], quasiperiodic partial synchronization (QPS) [22,36], as well as collective and microscopic chaos [21–24,26,30,33,36]. In a QPS state, see, e.g., Fig. 1(b), the mean field $\bar{A}$ rotates uniformly, while the individual oscillators behave quasiperiodically (since each oscillator "feels" the periodic driving of the mean field). Remarkably, increasing coupling QPS may undergo a couple of secondary Hopf bifurcations resulting in a state of pure collective chaos [24,36]. With this term we refer to a state in which the mean field behaves chaotically, while individual oscillators behave in seemingly chaoticlike fashion (neighboring oscillators remain close forever due to the absence of microscopic chaos). A shared feature of NUIS, QPS, and pure collective chaos [22,24,36] is that the relative positions of the oscillators on top of a closed curve are preserved; see Figs. 1(a), 1(b), and 1(c). This fact suggests that a description in terms of the oscillators' phases alone is possible.

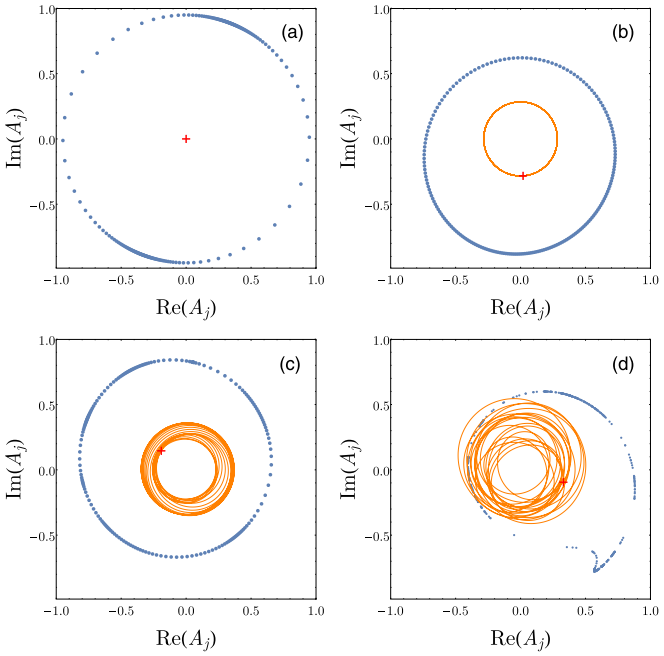

FIG. 1. Snapshot of the positions A_j for a population of $N = 200$ oscillators with $c_2 = 3$. The corresponding mean field $\bar{A}$ is marked by a red cross, and a thin solid line is the trajectory of $\bar{A}(t)$ for an interval of 50 t.u. (a) NUIS state with $Q \approx 0.755$ ($c_1 = -0.36$, $\epsilon = 0.1$). (b) Quasiperiodic partial synchrony ($c_1 = -2$, $\epsilon = 0.4135$). (c) Pure collective chaos ($c_1 = -2$, $\epsilon = 0.4165$). (d) Collective and microscopic chaos ($c_1 = -2$, $\epsilon = 0.47$) for $N = 500$.

In contrast to Fig. 1(c), Fig. 1(d) shows a chaotic regime in which phase description breaks down, as it involves microscopic degrees of freedom and no phase ordering exists. Hence, our ultimate goal is to find a phase-reduced model of Eq. (1) that captures as much as possible of the phase-describable states (NUIS, QPS, modulated QPS, pure collective chaos, etc.).

B. Basic phase diagrams

Before presenting our results, it is convenient to review previous results on the MF-CGLE. For fixed c_1 and c_2 values, let us denote by ϵ_s and ϵ_0 the ϵ values of marginal linear stability for FS and UIS. Closed formulas for ϵ_s and ϵ_0 are [21,22]

$$\epsilon_s = -\frac{2(1 + c_1 c_2)}{1 + c_1^2}, \quad (2)$$

$$\epsilon_0(2\epsilon_0 - 1)c_1^2 + 4(\epsilon_0 - 1)(2\epsilon_0 - 1)c_1 c_2 - \epsilon_0(\epsilon_0 - 1)c_2^2 + (3\epsilon_0 - 2)^2 = 0. \quad (3)$$

These formulas are also valid for finite ensembles, assuming ϵ_0 refers to the splay state. To visualize the stability

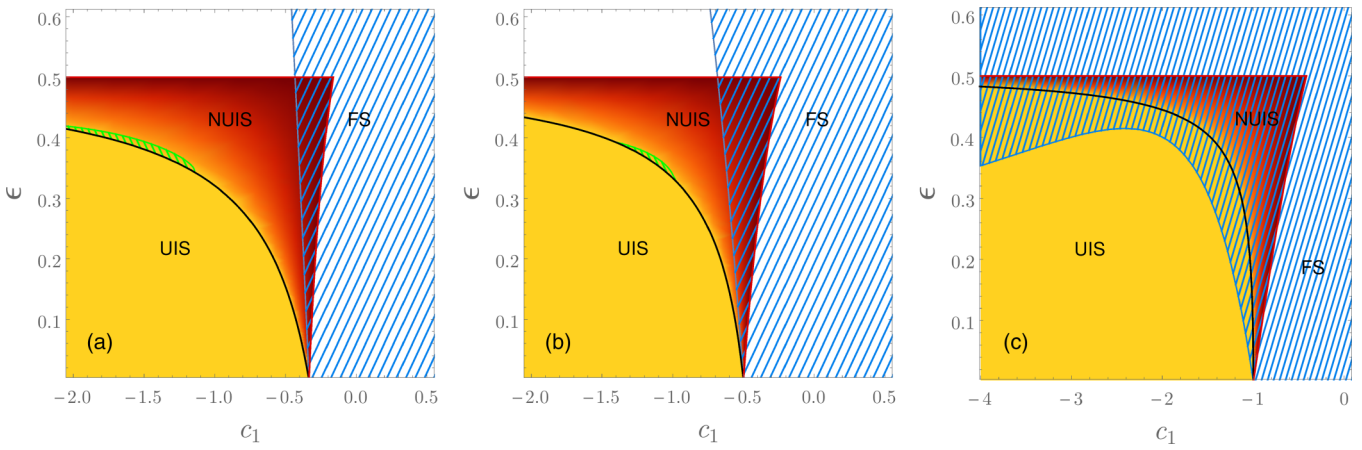

FIG. 2. Partial phase diagram of the MF-CGLE for $c_2 = 3$ (a), 2 (b), and 1 (c). In each panel, the region with stable UIS is depicted in yellow, and the region with color gradation corresponds to stable NUIS, with a color gradient that indicates the actual Q value (see the text); it becomes darker as $Q \to 1$. Stable FS is indicated by a blue hatched region. The stability boundaries of FS, UIS, and ($Q = 1$)-NUIS are depicted by blue, black, and red lines, respectively, following Eqs. (2), (3), and (4) (setting $Q = 1$). In panels (a) and (b), there is a green-hatched region where other phase-describable states such as the ones shown in Figs. 1(b) and 1(c) are stable.

boundaries in Eqs. (2) and (3), it is convenient to fix either c_1 or c_2. Following [22] we choose to fix c_2, and display the loci of ϵ_s and ϵ_0 in the parameter plane (c_1, ϵ). In the phase diagrams in Figs. 2(a), 2(b), and 2(c), we selected $c_2 = 3$, 2, and 1, respectively. This choice is motivated by the fact that most previous works on the MF-CGLE adopt either $c_2 = 2$ or 3. One key observation is that, as ϵ_s and ϵ_0 approach zero, the boundaries converge to the condition $1 + c_1 c_2 = 0$, which is the well known Benjamin-Feir-Newell criterion for the stability of uniform oscillations in the complex Ginzburg-Landau equation in arbitrary dimension [4,13,38,39]. There is a critical value $c_2 = \sqrt{3} = 1.732\ldots$ at which the boundaries ϵ_s and ϵ_0 become tangent at $\epsilon = 0$. Accordingly, for $c_2 = 1$, see Fig. 2(c), there is a region of bistability between UIS and synchrony, in contrast, e.g., to Fig. 2(b).

The stability of a NUIS depends exclusively on the mean field $Q = |N^{-1} \sum_j \exp(2i\varphi_j)|$. The coupling constant ϵ_Q at which one particular NUIS becomes unstable was obtained in Ref. [25]:

$$\begin{aligned}&\big[\epsilon_Q(2\epsilon_Q - 1)c_1^2 + 4(\epsilon_Q - 1)(2\epsilon_Q - 1)c_1 c_2\\ &-\epsilon_Q(\epsilon_Q - 1)c_2^2 + (3\epsilon_Q - 2)^2\big]\big[(2 - 3\epsilon_Q)^2 + \epsilon_Q^2 c_1^2\big]\\ &\quad = Q^2 \epsilon_Q (1 - \epsilon_Q)(3\epsilon_Q - 2)^2 \big(c_1^2 + 1\big)\big(c_2^2 + 1\big). \qquad (4)\end{aligned}$$

This formula is the generalization of (3) with the important qualitative information that the size of the stability region increases as Q grows, reaching its maximum for $Q = 1$. At $Q = 1$, the NUIS collapses into a two-cluster state with equally populated groups. The value of Q is still far from breaking the degeneracy of a NUIS, provided $Q \neq 1$, since the values of all "higher-order" mean fields $f_n = |N^{-1} \sum_j \exp(ni\varphi_j)|$ ($n > 2$) are free. Nevertheless, the conclusion based on numerical simulation is that any small amount of noise causes f_n to converge to zero, and Q to take the smallest value among all non-unstable (i.e., neutrally stable) NUISs. Therefore, it is assumed hereafter that the term NUIS is constrained to $f_n = 0$ ($n > 2$).

Figures 2(a) and 2(b) include a green-hatched region, adjacent to the UIS region at moderate ϵ values, where other phase-describable states are stable. These are QPS, modulated QPS, and pure-collective chaos [24,36]. We determined the boundary through simulations with $N = 200$ oscillators, but the result is insensitive if a larger N value is used.

C. First-order phase reduction: Kuramoto-Sakaguchi model

At the lowest order, applying the classical averaging technique [4,13,37] to Eq. (1) yields the Kuramoto-Sakaguchi model [40]. In this model, each oscillator is described by a phase θ_j, and it is coupled to the other ones by pairwise interactions of the form $\sin(\theta_i - \theta_j + \alpha)$. In agreement with the mean-field character of the system, oscillators are coupled through the Kuramoto order parameter $Z_1 \equiv R e^{i\Psi} = N^{-1} \sum_{k=1}^{N} e^{i\theta_k}$, such that the ordinary differential equations governing the dynamics are

$$\dot{\theta}_j = \Omega + \epsilon \eta R \sin(\Psi - \theta_j + \alpha), \qquad (5)$$

with constants $\Omega \equiv -c_2 + \epsilon(c_2 - c_1)$, $\eta \equiv \sqrt{(1 + c_2^2)(1 + c_1^2)}$, and phase lag

$$\alpha = \arg[1 + c_1 c_2 + (c_1 - c_2)i]. \qquad (6)$$

Equation (5) is the disorder-free version of the paradigmatic Kuramoto-Sakaguchi model [13,40] and related models [41]. The dynamics of Eq. (5) is determined by the sign of $1 + c_1 c_2$ (Benjamin-Feir-Newell criterion): full synchrony—corresponding to $R = 1$—is stable for $1 + c_1 c_2 > 0$, and unstable for $1 + c_1 c_2 < 0$. In the latter case, among infinitely many oscillator densities with $R = 0$, there is a convergence to the UIS under an arbitrarily weak noise [22].

As discussed above, the MF-CGLE has much richer dynamics than its first-order phase reduction (5), even arbitrarily close to the $\epsilon = 0$ limit. Therefore, it is mandatory to extend the phase reduction to order $O(\epsilon^2)$ if we wish to avoid degeneracies in the phase approximation. This is what we do next.

III. SYSTEMATIC PHASE REDUCTION

In spite of the relevance of Eq. (1), no phase reduction beyond the first order is currently available. Finding higher-order terms in the phase reduction is necessary to unfold the singularity at $(c_1, \epsilon) = (-1/c_2, 0)$; see Fig. 2. This path of investigation should allow us to discern which are the true behaviors of the MF-CGLE in the small-coupling limit $|\epsilon| \ll 1$. Moreover, it might serve to shed light on the mechanisms behind complex dynamics found (so far) for moderate ϵ values.

An isochron-based phase reduction approach is developed here. It allowed us to obtain the phase reduction of the MF-CGLE up to order ϵ^3. In this section, we give the details of our phase-reduction calculation. We anticipate that the results at second and third order in ϵ correspond to Eqs. (15) and (29) below.

A. Isochrons

The concept of isochron [42,43] is the cornerstone of phase-reduction methods [1,13]. Isochrons foliate the attraction basin of a stable limit cycle, each intersecting it at one point. The phase of that point is attributed to all points of the isochron, motivated by their convergence as time goes to infinity (the so-called "asymptotic phase" [44]). For the Stuart-Landau oscillator, polar coordinates (r, φ) relate to the phase θ according to [4,13]

$$\theta(r, \varphi) = \varphi - c_2 \ln r. \tag{7}$$

As mentioned above, on the limit cycle ($r = 1$), $\theta = \varphi$. The term "nonisochronicity" or "shear" for parameter c_2 becomes clear in light of Eq. (7), since c_2 controls how much the isochrons deviate from radial lines.

B. Isochron-based phase reduction

We continue the analysis writing Eq. (1) in polar coordinates:

$$\dot{r}_j = r_j\left(1 - \epsilon - r_j^2\right) + \frac{\epsilon}{N}\sum_{k=1}^{N} r_k[\cos(\varphi_k - \varphi_j) - c_1 \sin(\varphi_k - \varphi_j)], \tag{8}$$

$$\dot{\varphi}_j = -c_2 r_j^2 - \epsilon c_1 + \frac{\epsilon}{N r_j}\sum_{k=1}^{N} r_k[c_1 \cos(\varphi_k - \varphi_j) + \sin(\varphi_k - \varphi_j)]. \tag{9}$$

After the change of variables $(r_j, \varphi_j) \to (r_j, \theta_j)$ through Eq. (7), we get

$$\dot{r}_j = f(r_j) + \epsilon g_j(\mathbf{r}, \boldsymbol{\theta}), \tag{10a}$$

$$\dot{\theta}_j = \epsilon h_j(\mathbf{r}, \boldsymbol{\theta}). \tag{10b}$$

Here, we have also implemented the transformation $\theta_j \to \theta_j - c_2 t$ (by moving to a rotating frame with angular velocity $-c_2$). In this way, the time derivatives of the phases in (10b) are proportional to ϵ, while the r_j are fast variables that become enslaved to the dynamics of θ_j. In Eq. (10) $f(r) = r(1 - r^2)$, and functions g_j and h_j depend on the vectors $\mathbf{r} = (r_1, r_2, \ldots, r_N)^T$ and $\boldsymbol{\theta} = (\theta_1, \theta_2, \ldots, \theta_N)^T$ as follows:

$$g_j(\mathbf{r}, \boldsymbol{\theta}) = -r_j + \frac{1}{N}\sum_{k=1}^{N}\left\{r_k\left[\cos\left(\theta_k - \theta_j + c_2 \ln\frac{r_k}{r_j}\right) - c_1 \sin\left(\theta_k - \theta_j + c_2 \ln\frac{r_k}{r_j}\right)\right]\right\}, \tag{11a}$$

$$h_j(\mathbf{r}, \boldsymbol{\theta}) = c_2 - c_1 + \frac{1}{N r_j}\sum_{k=1}^{N}\left\{r_k\left[(c_1 - c_2)\cos\left(\theta_k - \theta_j + c_2 \ln\frac{r_k}{r_j}\right) + (1 + c_1 c_2)\sin\left(\theta_k - \theta_j + c_2 \ln\frac{r_k}{r_j}\right)\right]\right\}. \tag{11b}$$

The separation of time scales in Eq. (10) suggests using classical perturbation techniques such as averaging, adiabatic approximation, or two-timing. However, the perturbation approach described next proved to be both conceptually simple and much less convoluted, permitting us to obtain the phase reduction up to cubic order in ϵ. Based on the empirical observation that, at small ϵ values, the oscillators fall on a closed curve and preserve their phase ordering, we assume that the radii are completely determined by the phases $r_j = r_j(\theta_1, \theta_2, \ldots, \theta_N)$. We also postulate an expansion in powers of ϵ for the radii: $r = r_j^{(0)} + \epsilon r_j^{(1)} + \epsilon^2 r_j^{(2)} + \cdots$; or in vector notation, $\mathbf{r} = \mathbf{r}^{(0)} + \epsilon\mathbf{r}^{(1)} + \epsilon^2\mathbf{r}^{(2)} + \cdots$. Equation (10b) for θ_j becomes

$$\dot{\theta}_j = \epsilon h_j(\mathbf{r}^{(0)}, \boldsymbol{\theta}) + \epsilon^2(\nabla_r h_j(\mathbf{r}^{(0)}, \boldsymbol{\theta}))\cdot\mathbf{r}^{(1)} + \epsilon^3[(\nabla_r h_j(\mathbf{r}^{(0)}, \boldsymbol{\theta}))\cdot\mathbf{r}^{(2)} + (\mathbf{Mrr})_j] + \cdots, \tag{12}$$

where $\nabla_r \equiv (\partial_{r_1}, \partial_{r_2}, \ldots, \partial_{r_N})$ and $(\mathbf{Mrr})_j \equiv \frac{1}{2!}\sum_{k,l}\partial_{r_k}\partial_{r_l}h_j(\mathbf{r}^{(0)}, \boldsymbol{\theta})r_k^{(1)}r_l^{(1)}$. Now, the explicit dependence on the radii in (12) must be removed. This is accomplished equating both sides of (10a) at the same order. The order $O(\epsilon^0)$ yields $r_j^{(0)} = 1$, and (12) becomes (at the lowest order) the Kuramoto-Sakaguchi model (5). At order ϵ,

$$\dot{r}_j^{(1)} = f'\left(r_j^{(0)}\right)r_j^{(1)} + g_j(\mathbf{r}^{(0)}, \boldsymbol{\theta}). \tag{13}$$

As r_j depends exclusively on the phases, we can apply the chain rule: $\dot{r}_j = (\nabla_\theta r_j)\cdot\dot{\boldsymbol{\theta}}$. At order ϵ, the time derivative vanishes:

$$\dot{r}_j^{(1)} = \left(\nabla_\theta r_j^{(0)}\right)\cdot\mathbf{h} = \mathbf{0}.$$

Hence Eq. (13) yields the result

$$r_j^{(1)} = -\frac{g_j(\mathbf{r}^{(0)}, \boldsymbol{\theta})}{f'\left(r_j^{(0)}\right)} = \frac{g_j(\mathbf{r}^{(0)}, \boldsymbol{\theta})}{2}, \tag{14}$$

which can be inserted in (12) to obtain the ϵ^2 contribution. Through elementary manipulations, the second-order phase reduction of Eq. (1) can be condensed into this expression:

$$\dot{\theta}_j = \Omega + \epsilon\eta R\sin(\Psi - \theta_j + \alpha) + \frac{\epsilon^2\eta^2}{4}\left\{R Q\sin(\Phi - \Psi - \theta_j) - \sum_{m=1}^{2}(-R)^m\sin[m(\Psi - \theta_j) + \beta]\right\} + O(\epsilon^3). \tag{15}$$

The $O(\epsilon^2)$ term depends on Z_1 as well as on the second Kuramoto-Daido order parameter [45] $Z_2 \equiv Q\, e^{i\Phi} = N^{-1}\sum_{k=1}^{N} e^{2i\theta_k}$. To enhance the clarity of Eq. (15), we found it convenient to define a phase lag

$$\beta = \arg\left(1 - c_1^2 + 2c_1 i\right), \tag{16}$$

which turns out to be independent of c_2. The other constants in Eq. (15) are the same as in Eq. (5); as the change to a rotating frame has been reversed, the $O(\epsilon^0)$ term inside Ω is $-c_2$ (as before).

IV. SECOND-ORDER PHASE REDUCTION: THREE-BODY INTERACTIONS

In this section, we study in detail the phase model obtained from the second-order phase reduction of the MF-CGLE, i.e., the system of phase oscillators governed by Eq. (15). Of the three $O(\epsilon^2)$ contributions to Eq. (15), the first element of the sum ($m = 1$) entails a parameter shift to the $O(\epsilon)$ interaction, and it is therefore irrelevant in qualitative terms. The other two terms in Eq. (15) correspond to three-body (i.e., nonpairwise) interactions:

$$R^2 \sin[2(\Psi - \theta_j) + \beta] = \frac{1}{N^2}\sum_{k,l} \sin(\theta_k + \theta_l - 2\theta_j + \beta), \tag{17}$$

$$R\,Q \sin(\Phi - \Psi - \theta_j) = \frac{1}{N^2}\sum_{k,l} \sin(2\theta_k - \theta_l - \theta_j). \tag{18}$$

The price of working only with the phases is that two-body interactions of the original MF-CGLE (1) become multibody interactions, as higher orders of ϵ are considered. In comparison to Eq. (1), our phase model can be much more efficiently analyzed, both analytically and numerically. We devote the remainder of this section to analyze the phase model in Eq. (15). We note that, as expected, the model is invariant under global phase shift $\theta_j \to \theta_j + \phi$. For the sake of making the presentation simpler, we assume constant $\Omega = 0$, since this can always be achieved by going to a rotating frame $\theta_j \to \theta_j + \Omega t$.

A. Full synchronization

The stability boundary of FS ($\theta_j = \Psi = \Phi/2$) is easily calculated. In particular, for infinite N it is almost immediate: we simply assume one oscillator is infinitesimally perturbed, say the first one, $\theta_1 = \Psi + \delta\theta_1$. The evolution of the perturbation obeys the linear equation $d\delta\theta_1/dt = \epsilon\eta[\cos\alpha + \frac{\epsilon\eta}{4}(1 - \cos\beta)]\delta\theta_1$. At threshold ($d\delta\theta_1/dt = 0$) the coupling satisfies

$$\epsilon_s = \frac{-2(1 + c_1 c_2)}{c_1^2\left(1 + c_2^2\right)}, \tag{19}$$

where we have written $\cos\alpha$ and $\cos\beta$ in terms of c_1 and c_2. For illustration, the curve defined by (19) is represented by a blue dotted line in Figs. 3(a) and 3(b) for $c_2 = 3$ and $c_1 = 1$, respectively. Equation (19) is asymptotically exact as $\epsilon_s \to 0$, and deviates progressively from the FS boundary of the MF-CGLE (represented by a solid line) as ϵ_s increases.

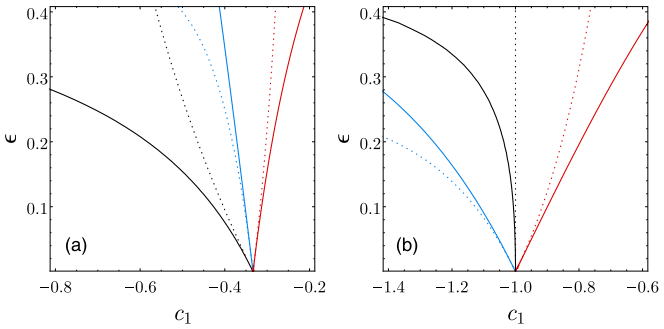

FIG. 3. Comparison between the bifurcation lines of FS, UIS, and NUIS ($Q = 1$) for the MF-CGLE (solid lines) and for the second-order phase reduction (dashed lines). Line colors are the same as in Fig. 2. (a) $c_2 = 3$ and (b) $c_2 = 1$.

B. Incoherent states

We adopt the thermodynamic limit and define a density ρ such that $\rho(\theta, t)d\theta$ is the fraction of oscillators with phases between θ and $\theta + d\theta$. Now $\theta \in [0, 2\pi)$ is a cyclic variable, i.e., $\rho(\theta + 2\pi, t) = \rho(\theta, t)$, and we impose the normalization condition $\int_0^{2\pi} \rho(\theta, t)d\theta = 1$. The oscillator density ρ obeys the continuity equation because of the conservation of the number of oscillators:

$$\partial_t \rho(\theta, t) + \partial_\theta[v(\theta)\rho(\theta, t)] = 0. \tag{20}$$

Here $v = \dot{\theta}$ is the ρ-dependent velocity of an oscillator with phase θ. We define the Fourier modes of ρ:

$$\rho(\theta, t) = \frac{1}{2\pi}\sum_{n=-\infty}^{\infty} \rho_n e^{in\theta}, \tag{21}$$

with $\rho_0 = 1$ and $\rho_n = \rho_{-n}^*$. The mean fields Z_n reduce to

$$Z_n = \int_0^{2\pi} \rho(\theta, t)\, e^{in\theta}\, d\theta = \rho_{-n}.$$

Inserting the Fourier expansion (21) into the continuity equation (20) allows us to rewrite our model in Fourier space:

$$\begin{aligned}\dot{\rho}_n = \frac{n}{2}\epsilon\eta\Big\{ & e^{-i\alpha}\rho_1\rho_{n-1} - e^{i\alpha}\rho_1^*\rho_{n+1} \\ & + \frac{\epsilon\eta}{4}[e^{-i\beta}\rho_1(\rho_{n-1} - \rho_1\rho_{n-2}) - e^{i\beta}\rho_1^*(\rho_{n+1} - \rho_1^*\rho_{n+2}) \\ & - \rho_2^*\rho_1\rho_{n+1} + \rho_2\rho_1^*\rho_{n-1}]\Big\}.\end{aligned} \tag{22}$$

1. Uniform incoherent state

The stability boundary of the UIS [$\rho(\theta) = (2\pi)^{-1} \Leftrightarrow \rho_{n\neq 0} = 0$] is obtained linearizing the previous equation. It is easy to notice that only the first mode may destabilize. We have for $|\rho_1| \ll 1$,

$$\frac{d}{dt}\delta\rho_1 = \frac{\epsilon\eta}{2}\left[e^{-i\alpha} + \frac{\epsilon\eta e^{-i\beta}}{4}\right]\delta\rho_1. \tag{23}$$

Neglecting the trivial marginal case $\epsilon = 0$, the stability boundary satisfies $\cos\alpha + (1/4)\epsilon_0\eta\cos\beta = 0$. Or in terms of c_1

and c_2,

$$\epsilon_0 = \frac{4(1+c_1c_2)}{(c_1^2-1)(1+c_2^2)}. \tag{24}$$

In Figs. 3(a) and 3(b), we can contrast this formula with the exact one for the MF-CGLE, Eq. (3), for two c_2 values.

2. *Nonuniform incoherent states*

According to (22), in an incoherent state ($\rho_1 = 0$) higher-order modes are at rest: $\dot{\rho}_n = 0$ ($n > 2$). The linearization of (22) around $\rho_1 = 0$ and $\rho_n \neq 0$ ($|n| \geqslant 2$) is (schematically) as follows:

$$\frac{d}{dt}\begin{pmatrix}\delta\rho_1\\ \delta\rho_1^*\\ \delta\rho_2\\ \delta\rho_2^*\\ \vdots\end{pmatrix} = \left(\begin{array}{cc|ccc} \bullet & \bullet & 0 & 0 & \cdots \\ \bullet & \bullet & 0 & 0 & \cdots \\ \hline \bullet & \bullet & 0 & 0 & \cdots \\ \bullet & \bullet & 0 & 0 & \cdots \\ \vdots & \vdots & \vdots & \vdots & \ddots \end{array}\right)\begin{pmatrix}\delta\rho_1\\ \delta\rho_1^*\\ \delta\rho_2\\ \delta\rho_2^*\\ \vdots\end{pmatrix}, \tag{25}$$

where the $\bullet$ symbols denote nonzero elements. Clearly, the structure of this equation yields an infinite set of vanishing eigenvalues plus two eigenvalues coming from the first two rows. The equation for $\delta\rho_1$ is hence the only relevant one. The linear terms in $\delta\rho_1$ yield

$$\dot{\delta\rho_1} = \frac{\epsilon\,\eta}{2}\left\{\left[e^{-i\alpha} + \frac{\epsilon\eta}{4}(e^{-i\beta} - |\rho_2|^2)\right]\delta\rho_1 - \left[e^{i\alpha} + \frac{\epsilon\eta}{4}(e^{i\beta} - 1)\right]\rho_2\,\delta\rho_1^*\right\}. \tag{26}$$

All higher-order modes, save ρ_2, are absent in the equation. As $\dot{\rho}_2 = 0$, we can choose the coordinate axes such that $\rho_2 = Q \in \mathbb{R}$. After some calculations, we find that NUIS with a specific Q value is marginally stable at

$$\epsilon_Q = \frac{4(1+c_1c_2)}{(c_1^2-1)(1+c_2^2)+\eta^2Q^2}. \tag{27}$$

As occurs in the MF-CGLE, the larger Q is, the larger is the stability region of the NUIS. Our empirical observation is that, for given c_1 and c_2, if ϵ is set at a certain $\epsilon = \epsilon_{Q^*}$ the numerical integration of the system (either oscillators or Fourier modes), under a very weak noise, always converges to a NUIS with $\rho_{n\geqslant 3} = 0$; and $|\rho_2| = Q^*$. In other words, the system adopts the minimum value of $|\rho_2|$ among all allowed by Eq. (27).

The state $Q = 1$ ($R = 0$)—the last NUIS to destabilize—is singular, not only because it is just a two-cluster state with two equally populated groups, but also because in contrast to the other NUIS, the instability is not oscillatory. Equation (26) takes the form $\dot{\delta\rho_1} \propto a\,\delta\rho_1 - a^*\,\delta\rho_1^*$, which yields an additional zero eigenvalue corresponding to the direction $\mathrm{Im}(\delta\rho_1) = 0$.

C. Validity and accuracy

From our previous results, we conclude that the phase reduction (15) is free of degeneracies. The boundaries of FS, UIS, and NUIS with different Q values do not overlap. As a double-check of the correctness of our analysis, we verified that the boundaries (19), (24), and (27) obtained through the phase reduction are tangent to the equivalent boundaries of the MF-CGLE, Eqs. (2), (3), and (4), at $\epsilon = 0$. In Fig. 3 we depict together the boundaries of FS, UIS, and ($Q = 1$)-NUIS of the MF-CGLE (solid lines) and phase reduction to second order (dashed lines) for two values of the nonisochronicity: $c_2 = 3$ and 1. These plots permit us to identify the range of ϵ in which the second-order approximation is accurate. For $c_2 = 1$ the approximate bifurcation lines are accurate up to $\epsilon \approx 0.05$, while this range is certainly smaller for $c_2 = 3$.

For general c_1, c_2 values, the prefactor $(\epsilon\eta)^n$ appearing for first ($n = 1$) and second ($n = 2$) orders suggests to extrapolate the relative smallness of ϵ to other c_1 and c_2 values. Thus, if in Fig. 3(b) accuracy is good up to $\epsilon\eta \approx 0.05\eta$, and $\eta \approx 2$, we propose

$$\epsilon\eta < 0.1 \tag{28}$$

as a conservative range of validity of the second-order approximation. Nevertheless, Eq. (28) must be regarded with some caution, since the third-order contribution to the phase-reduction expansion is not exactly proportional to $(\epsilon\eta)^3$; see Sec. V.

D. Quasiperiodic partial synchronization

The phenomenon of QPS was originally reported in the MF-CGLE [24] as a state emerging from the destabilization of the UIS, see Fig. 1(b), though its finding is usually attributed to a model of phase oscillators [46]. As mentioned above, in a QPS state the mean-field rotates uniformly, but individual oscillators behave quasiperiodically. Each oscillator passes periodically through a bottleneck located at the phase $\arg(\bar{A})$. The onset of QPS looks like a Hopf bifurcation undergone by the UIS, but this is not the case because of the infinitely many neutral directions pointing to nearby NUISs. It is also important to emphasize that stable QPS does not settle any time the UIS becomes unstable. As can be appreciated in Figs. 2(a) and 2(b), QPS is only observed at moderate ϵ values when entering inside the green hatched region. Otherwise, what we observe in the MF-CGLE is that the QPS state born at the instability of the UIS is a saddle. For parameter values with unstable UIS and FS—outside the green-hatched regions—initial conditions close to the UIS approach QPS for long time, eventually converging to one NUIS. If any small amount of noise is present, the NUIS with the lowest Q among the non-unstable ones is selected. The same behavior is displayed by the second-order phase reduction, Eq. (15); see Fig. 4. The logarithmic scaling of the residence times near QPS indicates a heteroclinic connection between UIS and QPS. The amplitude of the saddle QPS depends on the particular parameter values. The state of QPS progressively grows as we move away from the UIS stability boundary, finally colliding with FS ($|\rho_n| \to 1$) at the point where FS becomes stable.

All in all, these results confirm the correctness of our expansion, but at the same time prove the limitations of the second-order reduction, since the QPS attractor—found at moderate ϵ values, see Figs. 2(a) and 2(b)—is not reproduced.

E. Clustering

Clustering is a much studied phenomenon in oscillator ensembles [47]. In a clustered state, there are several groups

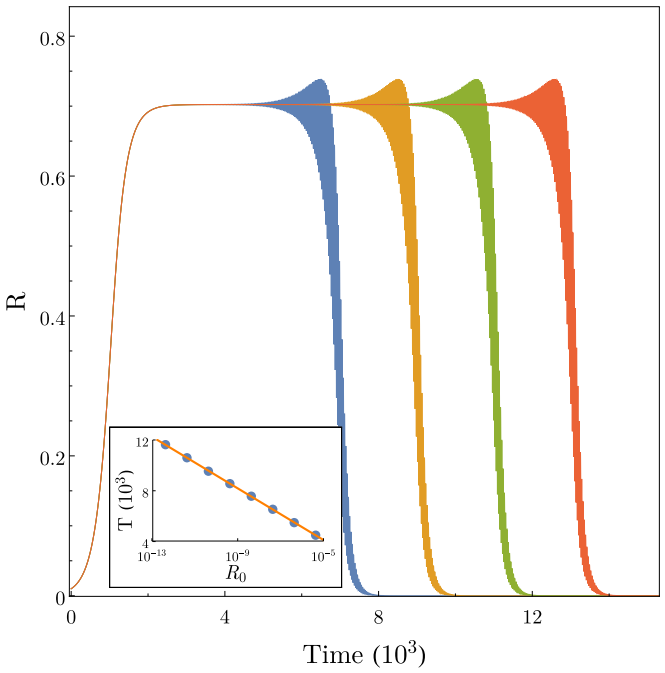

FIG. 4. Evolution of $R(t)$ for $N = 1000$ phase oscillators governed by (15) initiated near the UIS state. For the selected parameter values ($c_2 = 3$, $c_1 = -0.38$, $\epsilon = 0.1$), UIS is unstable but there are neutrally stable NUISs. After a transient in the neighborhood of QPS ($R(t) \approx$ const), the system approaches a particular NUIS ($R = 0$). From left to right, the initial conditions are random perturbations of the UIS with $R_0 = 4.3 \times \{10^{-7}, 10^{-9}, 10^{-11}, 10^{-13}\}$. The origin of times was shifted in all data sets to make the initial rise of R coincident. The inset shows the QPS transient time as a function of R_0. Note the logarithmic divergence of transient time $T \sim \ln R_0$ (consistent with heteroclinicity).

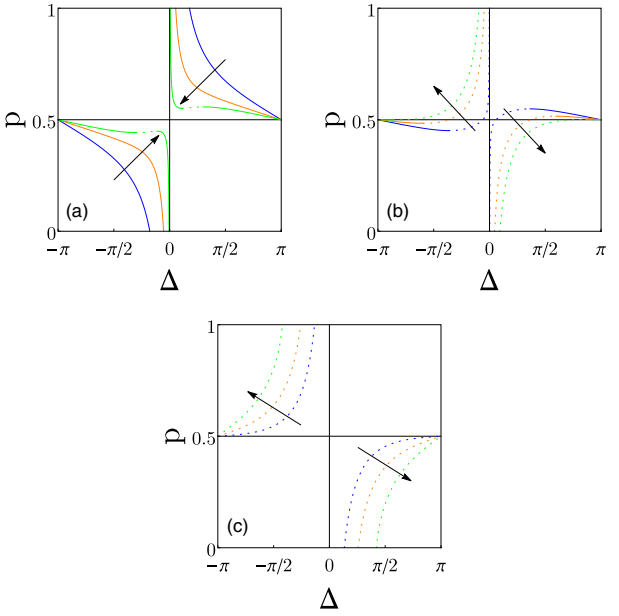

FIG. 5. Two-cluster solutions of Eq. (15). Each panel represents the fraction p of oscillators in one cluster as a function of the phase lag between clusters $\Delta = \theta^A - \theta^B$. We fix $c_2 = 3$ and $\epsilon = 0.3$ and select three values of c_1 in each panel. The arrow indicates the direction of increasing c_1. Solid (dashed) lines indicate stable (unstable) locking of the clusters. (a) Unstable FS region, $c_1 = -0.7, -0.5, -0.43$; (b) stable FS and not unstable ($Q = 1$)-NUIS region, $c_1 = -0.42, -0.36, -0.3$; (c) stable FS and unstable ($Q = 1$)-NUIS region, $c_1 = -0.25, -0.1, 0.1$.

of oscillators, each group formed by oscillators sharing the same phase. These kind of states are always possible in a mean-field model, so the relevant question is the stability. Indeed, the MF-CGLE is known to exhibit stable cluster at certain parameter ranges [21,22,27–29,33,35], specifically for strong coupling ($\epsilon \approx 1$).

Are there stable clustered states at small coupling? Our phase model allows us to address this question in an analytical way. Nonetheless, the general problem is intractable, and we decided to restrict our study to states with two point clusters, where a fraction p of the population is in the A-state θ^A, and the remaining $(1 - p)$ fraction is in the B-state $\theta^B \neq \theta^A$. We now summarize the results; the corresponding calculations can be found in Appendix A.

As an illustrative example, Fig. 5 depicts the combinations of phase difference $\Delta = \theta^A - \theta^B$ and imbalance p corresponding to actual cluster solutions for three different c_1 values with fixed values of c_2 and ϵ. Each panel is a typical situation in a specific region of parameter space. At the FS threshold, between panels (a) and (b), there is an infinity of two-cluster solutions colliding with FS ($\Delta = 0$). As a consequence, there is a reconnection of the two-cluster solutions. In Fig. 5, solid lines represent stable locking of the clusters. However, these solutions are fragile against disintegration of the largest cluster. Our conclusion after an extensive exploration of parameter space is that stable two-cluster states are not stable at small coupling. To be more precise, what we observe in our second-order phase reduction, Eq. (15), is that stable clustering is hardly found, and if so, it always requires moderate coupling strengths, violating (28). And indeed, we could not replicate clustering in the MF-CGLE for the parameter values predicted by Eq. (15).

The stability analysis of the two-cluster solutions also confirmed that slow switching [48]—a stable heteroclinic connection between two configurations of $\Delta = \theta^A - \theta^B$—is not possible.

F. Finite population, $N = 4$

This work focuses on the behavior of the MF-CGLE in the thermodynamic limit ($N \to \infty$). But the phase reduction (15) is valid for an arbitrary population size. In this section, we construct a bifurcation diagram for $N = 4$ oscillators, one size previously considered in the MF-CGLE context [35,49]. Here, this choice is motivated by the fact that in globally coupled systems this is the smallest size with a continuum of states with $R = 0$ [50], equivalent to the NUISs for $N = \infty$.

In analogy with its thermodynamic limit, the finite-N Kuramoto-Sakaguchi model has an exceptional transition between FS and the splay state at $1 + c_1 c_2 = 0$. This degeneracy can be broken down, for instance, adding higher-order harmonics to the (pairwise) interactions [51]. In our case, degeneracy is broken down by the three-body interactions of the second order in the phase-reduction expansion.

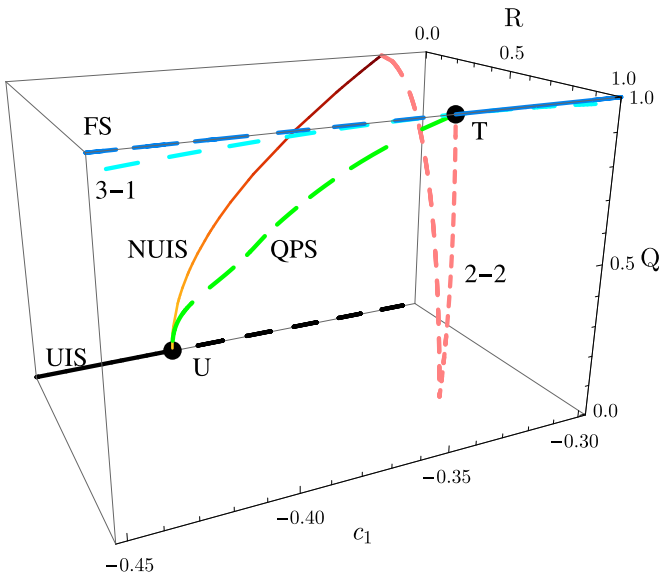

FIG. 6. Bifurcation diagram for Eq. (15) with $N = 4$ oscillators and $c_2 = 3$, $\epsilon = 0.1$. Solid (dashed) lines represent stable (unstable) solutions. In the case of UIS and NUIS, the solution depicted must be understood as the one observed under arbitrarily weak noise (there is a continuum of neutral solutions with Q larger than the solution depicted). The saddle QPS orbit was continued by means of a Newton-Raphson algorithm, and the values of R and Q assigned in the diagram correspond to their time averages.

Working with a small number of oscillators has the advantage that we can track all the stationary solutions, in particular the clustered solutions. As there are 3! orderings for the oscillator phases, and phase ordering is preserved by the dynamics because of the mean-field interactions, we choose the oscillators' labels such that $\theta_j \leqslant \theta_{j+1}$. (We assume here $\theta_j \in [0, 2\pi)$ to avoid artificial degeneracies.) The set of phases $\{\theta_1, \theta_2, \theta_3, \theta_4\}$ may take several invariant configurations. Apart from the trivial FS state $\{a, a, a, a\}$, there exists a continuum of "NUIS-like" $\mathbf{Z}_2$-symmetric states with $\{a, a + b, a + \pi, a + b + \pi\}$, where $b \in (0, \pi/2) \cup (\pi/2, \pi)$. In the limit $b \to \pi/2$, the NUIS becomes the splay state (the analog of UIS). In addition, in the limits $b \to 0$ and $b \to \pi$ the NUIS collapses into a two-cluster state with opposite phases. Apart from this one, other two-cluster solutions are possible. Namely, for some parameter values there exist two symmetry-related 2-2 configurations $\{a, a, b, b\}$ $(b \neq a + \pi)$. Additionally, one 3-1 cluster exists, designated as $\{a, a, a, b\}$ or $\{b, a, a, a\}$. Three-cluster solutions, like $\{a, a, b, c\}$, do not exist in our phase reduction, in contrast to the MF-CGLE for strong coupling [35]. Concerning the $N = 4$ analog of QPS, it is a periodic orbit, in which, due to the finiteness of the population, R and Q fluctuate around their average values.

We use R, Q, and c_1 to plot the bifurcation diagram in Fig. 6. These coordinates have the drawback of collapsing multiple equivalent states to a single point, hiding symmetries (e.g., pitchfork bifurcations). However, our choice intends to ease the comparison with the previous section, and with the same aim states are labeled borrowing the infinite-N terminology; namely, we use the labels UIS, NUIS, and QPS instead of splay state, $\mathbf{Z}_2$-symmetric state, and limit cycle, respectively.

Due to permutation symmetry FS destabilizes at point T in Fig. 6, as three eigenvalues go through zero simultaneously. This comprises an equivariant transcritical bifurcation with the 3-1 cluster, as well as a pitchfork bifurcation involving a 2-2 cluster. Moreover, at point T, QPS collapses into a heteroclinic cycle. This coincidence of bifurcations is a known scenario in systems with full permutation symmetry [50]. Concerning UIS, it undergoes an oscillatory instability at point U, but this is not a standard Hopf bifurcation because of the neutral direction along the NUIS manifold. QPS is a saddle, and not a stable limit cycle as might have been naively expected. In Fig. 6 we took $c_2 = 3$, and the QPS branch connects points T and U in a simple way. In contrast to Fig. 6, for $c_2 = 1$ FS and UIS coexist, and points U and T switch their relative positions. In that case the QPS branch is completely reversed (not shown), and the QPS solution is fully unstable. Consistently, we found a range of c_2 values in between, $1 < c_2 < 3$, where (depending on ϵ) the QPS branch develops a fold.

In summary, the bifurcation diagram for $N = 4$ appears to capture the global picture of the transition from UIS to FS. Considering more oscillators will increase the number of cluster solutions, see [27], but no essential new features.

V. THIRD-ORDER PHASE REDUCTION: FOUR-BODY INTERACTIONS

Our reason to deal with the third-order term now is to illustrate the practicality of the phase-reduction method, and get a glimpse of the power-series expansion at higher orders. Evaluating the cubic term in Eq. (12) yields the $O(\epsilon^3)$ correction to Eq. (15):

$$\begin{aligned}
&\epsilon^3 \frac{1 + c_2^2}{16} \{C_1 R \sin(\Psi - \theta_j + \gamma_1) \\
&\quad + C_2 R^2 \sin[2(\Psi - \theta_j) + \gamma_2] \\
&\quad + C_3 R\, Q \sin(\Phi - \Psi - \theta_j + \gamma_3) \\
&\quad + C_4 R\, Q^2 \sin(\Psi - \theta_j + \gamma_4) \\
&\quad + C_5 R^3 \sin(\Psi - \theta_j + \gamma_5) + C_6 R^2 Q \sin(\Phi - 2\theta_j + \gamma_6) \\
&\quad + C_7 R^3 \sin[3(\Psi - \theta_j) + \gamma_7] \\
&\quad + C_8 R^2 P \sin(\Xi - 2\Psi - \theta_j + \gamma_8) \\
&\quad + C_9 R^2 Q \sin(\Phi - 2\Psi + \gamma_9) + D R^2 \}. \qquad (29)
\end{aligned}$$

This expression depends on the third Kuramoto-Daido order parameter $Z_3 \equiv P e^{i\Xi} = N^{-1} \sum_j e^{i3\theta_j}$. The dependence of constants $\{C_j, \gamma_j\}_{j=1,\ldots,9}$ and D on c_1 and c_2 is tabulated in Appendix B. The structure of Eq. (29) deserves some words here. The terms proportional to C_j with indices $j = 1, 2, 3$ are higher-order corrections to Eq. (15), tantamount to a shift in parameter values. Four-body interactions appear in five different forms, corresponding to indices $j = 4, \ldots, 8$. For illustration, we expand a couple of these four-body

contributions:

$$R^3 \sin(\Psi - \theta_j) = \frac{1}{N^3} \sum_{k,l,n} \sin(\theta_k + \theta_l - \theta_n - \theta_j),$$

$$R^2 P \sin(\Xi - 2\Psi - \theta_j) = \frac{1}{N^3} \sum_{k,l,n} \sin(3\theta_k - \theta_l - \theta_n - \theta_j).$$

There are several qualitative features in Eq. (29) that deserve to be pointed out:

(i) The overall $O(\epsilon^3)$ contribution is not proportional to η^3—though some terms indeed are—in contrast to $O(\epsilon)$ and $O(\epsilon^2)$, which are proportional to η and η^2, respectively.

(ii) From Eqs. (15) and (29) we can expect that truncation of the power series to order ϵ^n yields up to $(n+1)$-body interactions, but not higher-order nonpairwise couplings. We can also expect that only Kuramoto-Daido order parameters Z_k with $k \leqslant n$ appear.

(iii) The last two terms in Eq. (29) are somewhat unexpected (nonetheless see [17]), since they depend on the mean fields Z_1 and Z_2, but not on θ_j itself. They are hence irrelevant concerning synchronization boundaries.

(iv) As occurs with the $O(\epsilon^2)$ term, FS and (N)UIS states are consistent with the MF-CGLE dynamics: (i) all terms in (29) are proportional to R ensuring that the contribution to the oscillators' frequencies vanishes in one incoherent state; (ii) in the FS state, the contribution also vanishes, as expected since the frequency of FS in the MF-CGLE varies linearly with ϵ. Accordingly, it holds that $D + \sum_j C_j \sin\gamma_j = 0$; cf. Appendix B.

Unfortunately, there is not a recognizable pattern in the new terms appearing in the power-series expansion, so it is not possible to extrapolate to higher orders in ϵ.

From Eqs. (15) and (29) we can derive the stability boundary of FS, NUIS (for UIS just set $Q = 0$) obtaining

$$2(1 + c_1c_2) + \epsilon_s c_1^2\left(1 + c_2^2\right) + \epsilon_s^2 c_1^3 c_2\left(1 + c_2^2\right) = 0, \quad (30)$$

$$4(1 + c_1c_2) + \epsilon_Q\left(1 + c_2^2\right)\left[\left(1 - c_1^2\right) - Q^2\left(1 + c_1^2\right)\right] + \frac{\epsilon_Q^2}{2}\left(1 + c_2^2\right)\left[\left(2 - 2c_1^2 - 3c_1c_2 + c_1^3c_2\right) - Q^2\left(1 + c_1^2\right)(-2 + 3c_1c_2)\right] = 0. \quad (31)$$

In Fig. 7 we depict (a) ϵ_0 and (b) ϵ_s from the previous expressions and compare them with the result of the MF-CGLE, and with the second-order approximation. The slopes and the curvatures of the bifurcation lines of the third-order phase reduction agree with those of the MF-CGLE at $\epsilon = 0$.

VI. DISCUSSION

A. Alternative phase reduction(s)

Our phase reduction is a genuine power series in the small parameter ϵ. Another strategy to analyze (1) is to absorb the ϵA_j term prior to the phase reduction. Specifically, setting $t' = (1 - \epsilon)t$ and

$$\kappa = \frac{\epsilon}{1 - \epsilon}, \quad (32)$$

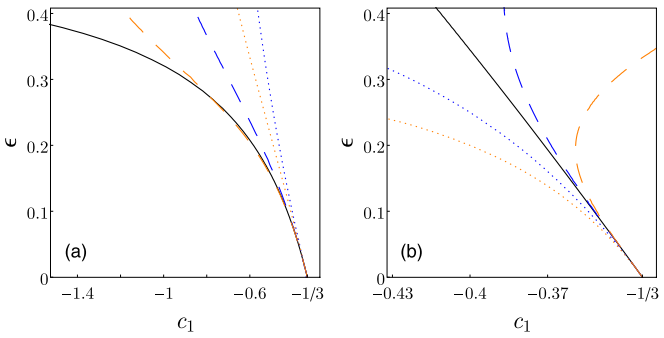

FIG. 7. Stability boundaries of (a) UIS and (b) FS obtained exactly and from phase approximations, for $c_2 = 3$. The solid line corresponds to the exact boundary of the MF-CGLE (1), while dotted and dashed lines correspond to second- and third-order phase approximations, respectively. Blue lines are obtained from (15) and (29). Orange lines are the results if prior to phase reduction the MF-CGLE is transformed into (33), performing an isochron-base phase reduction in powers of κ.

we get

$$\frac{dB_j}{dt'} = B_j - (1 + ic_2)|B_j|^2 B_j + \kappa(1 + ic_1)\bar{B}, \quad (33)$$

where $B_j = A_j \exp(i\epsilon c_1 t)/\sqrt{1 - \epsilon}$. Applying our phase-reduction method to (33) we obtain an alternative phase reduction in powers of κ (the result is not qualitatively different).

Is it worth transforming (1) into (33)? In other words, is the phase reduction of (33) up to order κ^n superior to that of (1) at order ϵ^n? Certainly, phase reductions at order ϵ^n and κ^n are not equivalent since $\kappa = \epsilon + \epsilon^2 + \epsilon^3 + \cdots$. Any truncation at order κ^n involves all powers of ϵ. The relative accuracy of the phase reductions of (33) and (1) at the same order can be assessed comparing the bifurcation loci. Instead of applying phase reduction to Eq. (33), the quickest strategy is to assume the existence of an exact phase reduction involving all orders in ϵ such that the exact critical value ϵ_* (the asterisk denotes an arbitrary state: UIS, FS,...) satisfies

$$\sum_{n=1}^{\infty} a_n(c_1, c_2)\,\epsilon_*^n + 1 + c_1c_2 = 0. \quad (34)$$

The coefficients a_n depend on the specific instability we are considering.

Phase reduction of (1) up to order n results in a truncation of (34) to order $n - 1$. For instance, the second-order phase reduction of (1) yields the linear relation [recall Eq. (19) or (24)]

$$a_1\epsilon_* + 1 + c_1c_2 = 0. \quad (35)$$

At the same order, the phase reduction of (33) results in an analogous expression

$$a_1'\kappa_* + 1 + c_1c_2 = 0. \quad (36)$$

Given that $\kappa = \epsilon + O(\epsilon^2)$, consistency with (34) determines $a_1' = a_1$. Thus the bifurcation locus estimated from the phase reduction of (33) satisfies (in coordinate ϵ) $a_1\epsilon_*/(1 - \epsilon_*) + (1 + c_1c_2) = 0$, which is slightly different from (35). Analogous reasoning permits us to obtain the bifurcation lines for

the third-order phase reduction of (33) from Eqs. (30) and (31).

A comparison of the bifurcations lines of UIS and FS is displayed in Figs. 7(a) and 7(b) for $c_2 = 3$. We see that the transformation of (1) into (33) allows us to obtain a phase model that captures better the stability boundary of UIS, but not of FS. It is easy to understand why. Each strategy captures better the dynamics in which the quantities multiplying the coupling constant are small. Thus, Eq. (1) is already a good starting point for states close to FS ($A_j \approx \bar{A}$), while (33) works better close to incoherence ($\bar{A} \approx \bar{B} \approx 0$). Finally, note that in addition to (1) and (33), there exists a continuum of alternative, intermediate formulations in which ϵA_j is only partly absorbed by a coordinate transformation.

B. Possible extensions of this work

The phase-reduction procedure presented in this work can be easily implemented in other geometries, different from the fully connected network. In a networked architecture, phase reduction at first order in ϵ couples phases with the nearest-neighbor phases. At order ϵ^2, second nearest neighbors come also into play [19], and progressively more distant nodes participate in the phase dynamics at higher orders. Also, the case of nonlocally coupled Stuart-Landau oscillators [52] is analyzable with the phase reduction presented here. Concerning the original complex Ginzburg-Landau equation, a partial differential equation of reaction-diffusion type, our phase reduction procedure is very simple and efficient obtaining the coefficients of the second-order terms: $\nabla^4\theta$, $(\nabla^2\theta)^2$, $(\nabla\theta)^2\nabla^2\theta$, $\nabla\theta\nabla^3\theta$ [13].

Concerning the oscillator dynamics, the phase reduction carried out here can be easily applied to planar oscillators with polar symmetry ($\lambda - \omega$ systems). In the latter case, analogously to (7), the isochrons satisfy $\theta = \varphi + \chi(r)$ [1]. Even if function χ does not have a closed form, it is still possible to obtain the phase model using the derivatives of the isochrons on the limit cycle.

C. Relationship with other phase-reduction approaches

In this subsection, we comment on the progress of our phase-reduction approach with respect to previous works, even if only directly applicable to $\lambda - \omega$ systems.

An alternative way of obtaining the second-order phase reduction of the MF-CGLE, Eq. (15), is applying the systematic averaging formulation in Chap. 4 of the book by Kuramoto [13]. This calculation is, however, much more lengthy than the one presented in Sec. III. Not surprisingly, obtaining the order ϵ^3 with the averaging approach [13] is a totally impractical task, while we succeeded with our method (with the assistance of symbolic software); see Eq. (29).

Equation (15) can also be obtained assuming small variations of the radii, i.e., setting $\dot{r}_j = 0$. This procedure was followed in [12,53], with the difference being that there the small quantities are deviations from the reference limit cycle. Here, we pursued a *bona fide* power expansion in terms of the coupling constant ϵ, and the result differs from the one obtained following [12,53]. In passing, we mention that instead of assuming $r_j = r_j(\theta_1, \theta_2, \ldots, \theta_N)$, once Eqs. (10) are derived, the two-timing approximation, such that the θ_j depend only on a slow time $\tau = \epsilon t$, can also be applied.

In contrast to our work, Refs. [17,54] apply first-order phase reduction obtaining multibody phase interactions. The reason is that those works invoke amplitude equations for an ensemble close (but not asymptotically close) to a Hopf bifurcation. The amplitude equation, which can be seen as a generalization of Eq. (1), turns out to contain nonlinear interactions. The nonlinear coupling among the A_j's leads to multibody interactions in the first-order phase reduction. Applying second-order phase reduction, as described here, to the amplitude equations in [17] or [54] may be interesting.

D. Toward a minimal phase model of pure collective chaos

Pure collective chaos has been found in several phase models with heterogeneity [55] or delay [56]. Collective chaos in the MF-CGLE, see Fig. 1(c), calls for a phase description in terms of identical phase oscillators (without delays). The fact that we have not found evidence of collective chaos in our numerical simulations of the second-order phase reduction (15)—nor in the third-order one—can be reasonably attributed to a too restrictive truncation of the power expansion. We believe that a higher-order truncation will capture better the behavior of the system at larger ϵ values, and eventually will exhibit collective chaos.

As pairwise interactions through higher harmonics, like $Q\sin(\Phi - 2\theta_j) = N^{-1}\sum_k \sin[2(\theta_k - \theta_j)]$, do not show up in the phase reduction of the MF-CGLE [57], multibody phase interactions appear to be the most promising ingredient to model collective chaos. In small ensembles of identical phase oscillators, higher harmonics as well as multibody interactions promote chaos alike; see [58] and [59], respectively. However, so far, collective chaos remains elusive in populations of higher-order pairwise interacting identical phase oscillators [60]. We believe multibody interactions could be the key element of collective chaos instead.

In the MF-CGLE with parameter values close to those in Fig. 1(c), we found chaos with a population size as small as $N = 6$. Does this say something about the order of the multibody interactions needed in the phase reduction? Is this chaos connected to collective chaos in the thermodynamic limit, as in [55]?

E. Conclusions

Multibody interactions are an unavoidable consequence of phase reduction, but save for a few works [12,16,59,61,62], the role of multibody phase interactions shaping exotic dynamics remains largely unexplored. In the weak-coupling regime of the MF-CGLE, multibody phase interactions are essential to describe *all* states apart from FS and UIS.

In summary, in this work we achieve second- and third-order phase reductions of the MF-CGLE. In our view, higher-order phase reductions promise to be crucial for our understanding of collective chaos and other exotic phenomena [12]. Moreover, analytic higher-order phase reductions may also serve as test beds for numerical phase reductions recently implemented [63]. For these reasons, we regard phase

reduction beyond the first order as an exciting battleground of nonlinear dynamics.

ACKNOWLEDGMENTS

We acknowledge support by MINECO (Spain) under Project No. FIS2016-74957-P. I.L. acknowledges support by Universidad de Cantabria and Government of Cantabria under the Concepción Arenal programme.

APPENDIX A: CLUSTERING

Our model (15) in a more convenient form (recall that in the rotating frame $\Omega = 0$) reads

$$\dot{\theta}_i = \frac{1}{N}\sum_j \Gamma(\theta_j - \theta_i) + \frac{1}{N^2}\sum_{j,k}[G_1(\theta_j + \theta_k - 2\theta_i) + G_2(2\theta_j - \theta_k - \theta_i)], \tag{A1}$$

with

$$\Gamma(x) = \epsilon[(c_1 - c_2)\cos x + (1 + c_1 c_2)\sin x] - G_1(x), \tag{A2}$$

$$G_1(x) = -\epsilon^2\left(1 + c_2^2\right)\left[\frac{c_1}{2}\cos x + \frac{\left(1 - c_1^2\right)}{4}\sin x\right], \tag{A3}$$

$$G_2(x) = \frac{\epsilon^2\left(1 + c_2^2\right)\left(1 + c_1^2\right)}{4}\sin x. \tag{A4}$$

Note that G_2 is an odd function.

Let us write first the evolution equation for cluster-A phase θ^A, defining the phase difference $\Delta = \theta^A - \theta^B$:

$$\begin{aligned}\dot{\theta}^A = {} & [p\Gamma(0) + (1-p)\Gamma(-\Delta)] \\ & + [p^2 G_1(0) + 2p(1-p)G_1(-\Delta) + (1-p)^2 G_1(-2\Delta)] \\ & + [-p(1-p)G_2(2\Delta) + (-2p^2 + 3p - 1)G_2(\Delta)];\end{aligned} \tag{A5}$$

the equivalent equation for the B-cluster is obtained with the substitution $\Delta \to -\Delta$ and $p \to (1-p)$. The evolution of $\Delta(t)$ obeys

$$\begin{aligned}\dot{\Delta} = {} & (2p-1)\Gamma(0) + (1-p)\Gamma(-\Delta) - p\Gamma(\Delta) \\ & + [-2p(1-p)G_2(2\Delta) + (-4p^2 + 4p - 1)G_2(\Delta)] \\ & + \{(2p-1)G_1(0) + 2p(1-p)[G_1(-\Delta) - G_1(\Delta)] \\ & + (1-p)^2 G_1(-2\Delta) - p^2 G_1(2\Delta)\}.\end{aligned} \tag{A6}$$

Setting $\dot{\Delta} = 0$ we obtain a quadratic equation in p that can be solved explicitly. We depict $p(\Delta)$ in Fig. 5 for selected parameter values. Note the symmetry of the curves because of the invariance under $(\Delta, p) \leftrightarrow (-\Delta, 1-p)$. There are Δ values for which p is out of the range (0,1), indicating no two-cluster states with those particular Δ values exist. Conversely, different values of Δ may be consistent with the same p value, indicating the coexistence of multiple two-cluster solutions with the same sizes.

1. Stability

First of all, note that one zero eigenvalue is always present due to the global phase shift invariance of the model, $\theta_j \to \theta_j + \text{const}$, and we ignore it hereafter. For the analysis that follows it is simpler to assume the thermodynamic limit (eigenvalues are the same for finite N, but the calculation is more convoluted.) As already known from previous studies [64], perturbations on a two-cluster solution can be decomposed in three orthogonal modes. Two of them are the disintegration of each respective cluster, and the third one is the unlocking of the two clusters. We denote λ_A, λ_B, and λ_L the corresponding eigenvalues. For the stability of the A-cluster, we need to evaluate if one oscillator in the neighborhood of this cluster decays to it or departs (i.e., "evaporates"). The eigenvalue λ_A is simply obtained linearizing around the state. The result is

$$\begin{aligned}\lambda_A = {} & -p\Gamma'(0) - (1-p)\Gamma'(-\Delta) - 2p^2 G_1'(0) \\ & - 4p(1-p)G_1'(-\Delta) - 2(1-p)^2 G_1'(-2\Delta) \\ & - p^2 G_2'(0) - (1-p)G_2'(\Delta) - p(1-p)G_2'(2\Delta).\end{aligned} \tag{A7}$$

The eigenvalue λ_B is obtained from λ_A after the substitution $p \to (1-p)$ and $\Delta \to -\Delta$, and vice versa. Finally, the locking between the clusters is controlled by the eigenvalue obtained linearizing (A6):

$$\begin{aligned}\lambda_L = {} & -(1-p)\Gamma'(-\Delta) - p\Gamma'(\Delta) - 2(1-p)^2 G_1'(-2\Delta) \\ & - 2p(1-p)[G_1'(-\Delta) + G_1'(\Delta)] - 2p^2 G_1'(2\Delta) \\ & - (4p^2 - 4p + 1)G_2'(\Delta) - 4p(1-p)G_2'(2\Delta).\end{aligned} \tag{A8}$$

Stability requires $\lambda_A, \lambda_B, \lambda_L < 0$. For small ϵ we summarized our findings in the main text, distinguishing three different regions corresponding to the three panels of Fig. 5. As said in the main text, we found stable clusters in the first region (FS unstable), e.g., $\epsilon = 0.1$, $c_1 = -9$, $c_2 = 2$. However, for these parameters the condition (28) does not hold, and in fact the cluster solution destabilized when we implemented it in the MF-CGLE.

2. No slow switching

With unstable two-cluster states, the system might still exhibit one nontrivial phenomenon called slow switching [48]. In this phenomenon, the clusters switch between two different Δ values with identical p value. The explanation for this behavior is a stable heteroclinic connection between the pair of two-cluster states that causes the system to switch forever between them with increasing residence times [48,64]. In practice [60], switching either terminates in one of the unstable two-cluster states (due to round-off errors), or it achieves a constant periodic switching (due to small noise). According to [64], slow switching requires the coexistence of three two-cluster states Δ', Δ'', and Δ''' with an identical p value, such that $0 < \Delta' < \Delta''' < \Delta'' < 2\pi$ and $\lambda_L < 0$ for Δ' and Δ'' while $\lambda_L > 0$ for Δ'''. As may be seen in Fig. 5, finding parameter values with three solutions for Δ at the same p is already difficult—only for the green line in Fig. 5(a) do such p values exist. In addition, the condition for the eigenvalues is even more stringent: e.g., in Fig. 5(a) the three points share

the stability of λ_A and λ_B making the heteroclinic connection impossible.

APPENDIX B: CONSTANTS C_j, γ_j, AND D IN EQ. (29)

The dependence of constants $\{C_j, \gamma_j\}_{j=1,\dots,9}$ and D on c_1 and c_2 is tabulated as follows:

$$C_j = \sqrt{A_j^2 + B_j^2}, \tag{B1}$$

$$\gamma_j = \arg(A_j + iB_j), \tag{B2}$$

where

$$\begin{aligned}
A_1 &= 2\big(c_2c_1^3 - 2c_1^2 - 3c_2c_1 + 2\big),\\
A_2 &= -\big(3c_1^3c_2 - 7c_1^2 - 9c_1c_2 + 5\big),\\
A_3 &= -2\big(c_1^2 + 1\big)(2c_1c_2 - 3),\\
A_4 &= 2\big(c_1^2 + 1\big)(c_1c_2 + 1),\\
A_5 &= 2\big(-c_2c_1^3 + c_1^2 + 2c_2c_1\big),\\
A_6 &= 3\big(c_1^2 + 1\big)(c_1c_2 - 1),\\
A_7 &= -\tfrac{1}{2}\big(-5c_2c_1^3 + 9c_1^2 + 15c_2c_1 - 3\big),\\
A_8 &= \tfrac{1}{2}\big(1 + c_1^2\big)(5c_1c_2 - 1),\\
A_9 &= \big(1 + c_1^2\big)(1 + c_1c_2),
\end{aligned}$$

and

$$\begin{aligned}
B_1 &= 2\big(4c_1 + c_2 - 3c_1^2c_2\big),\\
B_2 &= \big(c_1^3 + 9c_1^2c_2 - 11c_1 - 3c_2\big),\\
B_3 &= 2c_1\big(c_1^2 + 1\big),\\
B_4 &= 2\big(c_1^2 + 1\big)(c_1 - c_2),\\
B_5 &= \big(c_1^3 + 5c_2c_1^2 - c_1 - c_2\big),\\
B_6 &= -3\big(c_1^2 + 1\big)(c_1 + c_2),\\
B_7 &= \tfrac{1}{2}\big(-3c_1^3 - 15c_2c_1^2 + 9c_1 + 5c_2\big),\\
B_8 &= \tfrac{1}{2}\big(c_1^2 + 1\big)(c_1 + 5c_2),\\
B_9 &= \big(1 + c_1^2\big)(c_2 - c_1).
\end{aligned}$$

Additionally,

$$D = \big(c_1^2 + 1\big)(c_2 - c_1). \tag{B3}$$

[1] A. T. Winfree, *The Geometry of Biological Time* (Springer, New York, 1980).

[2] F. C. Hoppensteadt and E. M. Izhikevich, *Weakly Connected Neural Networks* (Spinger-Verlag, New York, 1997).

[3] S. H. Strogatz, *Sync: The Emerging Science of Spontaneous Order* (Hyperion, New York, 2003).

[4] A. S. Pikovsky, M. G. Rosenblum, and J. Kurths, *Synchronization, a Universal Concept in Nonlinear Sciences* (Cambridge University Press, Cambridge, 2001).

[5] D. Mertens and R. Weaver, Synchronization and stimulated emission in an array of mechanical phase oscillators on a resonant support, Phys. Rev. E **83**, 046221 (2011); Individual and collective behavior of vibrating motors interacting through a resonant plate, Complexity **16**, 45 (2011).

[6] I. Z. Kiss, C. G. Rusin, H. Kori, and J. L. Hudson, Engineering complex dynamical structures: Sequential patterns and desynchronization, Science **316**, 1886 (2007).

[7] J. F. Totz, R. Snari, D. Yengi, M. R. Tinsley, H. Engel, and K. Showalter, Phase-lag synchronization in networks of coupled chemical oscillators, Phys. Rev. E **92**, 022819 (2015).

[8] K. Wiesenfeld and J. W. Swift, Averaged equations for Josephson junction series arrays, Phys. Rev. E **51**, 1020 (1995).

[9] K. Wiesenfeld, P. Colet, and S. H. Strogatz, Synchronization Transitions in a Disordered Josephson Series Array, Phys. Rev. Lett. **76**, 404 (1996).

[10] A. A. Temirbayev, Z. Zh. Zhanabaev, S. B. Tarasov, V. I. Ponomarenko, and M. Rosenblum, Experiments on oscillator ensembles with global nonlinear coupling, Phys. Rev. E **85**, 015204(R) (2012).

[11] L. Q. English, Z. Zeng, and D. Mertens, Experimental study of synchronization of coupled electrical self-oscillators and comparison to the Sakaguchi-Kuramoto model, Phys. Rev. E **92**, 052912 (2015).

[12] M. H. Matheny, J. Emenheiser, W. Fon, A. Chapman, A. Salova, M. Rohden, J. Li, M. Hudoba de Badyn, M. Pósfai, L. Duenas-Osorio, M. Mesbahi, J. P. Crutchfield, M. C. Cross, R. M. D'Souza, and M. L. Roukes, Exotic states in a simple network of nanoelectromechanical oscillators, Science **363**, eaav7932 (2019).

[13] Y. Kuramoto, *Chemical Oscillations, Waves, and Turbulence* (Springer-Verlag, Berlin, 1984).

[14] H. Nakao, Phase reduction approach to synchronisation of nonlinear oscillators, Contemp. Phys. **57**, 188 (2016).

[15] B. Monga, D. Wilson, T. Matchen, and J. Moehlis, Phase reduction and phase-based optimal control for biological systems: A tutorial, Biol. Cybern. **113**, 11 (2019).

[16] T. Tanaka and T. Aoyagi, Multistable Attractors in a Network of Phase Oscillators with Three-Body Interactions, Phys. Rev. Lett. **106**, 224101 (2011).

[17] P. Ashwin and A. Rodrigues, Hopf normal form with S_N symmetry and reduction to systems of nonlinearly coupled phase oscillators, Physica D **325**, 14 (2016).

[18] M. Rosenblum and A. Pikovsky, Self-Organized Quasiperiodicity in Oscillator Ensembles with Global Nonlinear Coupling, Phys. Rev. Lett. **98**, 064101 (2007).

[19] B. Kralemann, A. Pikovsky, and M. Rosenblum, Reconstructing phase dynamics of oscillator networks, Chaos **21**, 025104 (2011); Reconstructing effective phase connectivity of oscillator networks from observations, New J. Phys. **16**, 085013 (2014).

[20] A. Pikovsky and M. Rosenblum, Dynamics of globally coupled oscillators: Progress and perspectives, Chaos **25**, 097616 (2015).

[21] V. Hakim and W. J. Rappel, Dynamics of the globally coupled complex Ginzburg-Landau equation, Phys. Rev. A **46**, R7347 (1992).

[22] N. Nakagawa and Y. Kuramoto, Collective chaos in a population of globally coupled oscillators, Prog. Theor. Phys. **89**, 313 (1993).

[23] N. Nakagawa and Y. Kuramoto, From collective oscillations to collective chaos in a globally coupled oscillator system, Physica D **75**, 74 (1994).

[24] N. Nakagawa and Y. Kuramoto, Anomalous lyapunov spectrum in globally coupled oscillators, Physica D **80**, 307 (1995).

[25] M.-L. Chabanol, V. Hakim, and W.-J. Rappel, Collective chaos and noise in the globally coupled complex Ginzburg-Landau equation, Physica D **103**, 273 (1997).

[26] M. Banaji and P. Glendinning, Towards a quasi-periodic mean field theory for globally coupled oscillators, Phys. Lett. A **251**, 297 (1999).

[27] M. Banaji, Clustering in globally coupled oscillators, Dyn. Syst. **17**, 263 (2002).

[28] H. Daido and K. Nakanishi, Diffusion-Induced Inhomogeneity in Globally Coupled Oscillators: Swing-by Mechanism, Phys. Rev. Lett. **96**, 054101 (2006).

[29] H. Daido and K. Nakanishi, Aging and clustering in globally coupled oscillators, Phys. Rev. E **75**, 056206 (2007).

[30] K. A. Takeuchi, F. Ginelli, and H. Chaté, Lyapunov Analysis Captures the Collective Dynamics of Large Chaotic Systems, Phys. Rev. Lett. **103**, 154103 (2009).

[31] K. A. Takeuchi and H. Chaté, Collective lyapunov modes, J. Phys. A **46**, 254007 (2013).

[32] G. C. Sethia and A. Sen, Chimera States: The Existence Criteria Revisited, Phys. Rev. Lett. **112**, 144101 (2014).

[33] W. L. Ku, M. Girvan, and E. Ott, Dynamical transitions in large systems of mean field-coupled Landau-Stuart oscillators: Extensive chaos and cluster states, Chaos **25**, 123122 (2015).

[34] M. Rosenblum and A. Pikovsky, Two types of quasiperiodic partial synchrony in oscillator ensembles, Phys. Rev. E **92**, 012919 (2015).

[35] F. P. Kemeth, S. W. Haugland, and K. Krischer, Cluster singularity: The unfolding of clustering behavior in globally coupled Stuart-Landau oscillators, Chaos **29**, 023107 (2019).

[36] P. Clusella and A. Politi, Between phase and amplitude oscillators, Phys. Rev. E **99**, 062201 (2019).

[37] Y. Kuramoto, Self-entrainment of a population of coupled nonlinear oscillators, in *International Symposium on Mathematical Problems in Theoretical Physics*, Lecture Notes in Physics Vol. 39, edited by H. Araki (Springer, Berlin, 1975), pp. 420–422.

[38] D. Walgraef, *Spatio-Temporal Pattern Formation* (Springer-Verlag, New York, 1997).

[39] I. S. Aranson and L. Kramer, The world of the complex Ginzburg-Landau equation, Rev. Mod. Phys. **74**, 99 (2002).

[40] H. Sakaguchi and Y. Kuramoto, A soluble active rotator model showing phase transitions via mutual entrainment, Prog. Theor. Phys. **76**, 576 (1986).

[41] E. Montbrió and D. Pazó, Collective synchronization in the presence of reactive coupling and shear diversity, Phys. Rev. E **84**, 046206 (2011); Shear Diversity Prevents Collective Synchronization, Phys. Rev. Lett. **106**, 254101 (2011); D. Pazó and E. Montbrió, The Kuramoto model with distributed shear, Europhys. Lett. **95**, 60007 (2011).

[42] A. T. Winfree, Patterns of phase compromise in biological cycles, J. Math. Biol. **1**, 73 (1974).

[43] J. Guckenheimer, Isochrons and phaseless sets, J. Math. Biol. **1**, 259 (1975).

[44] E. A. Coddington and N. Levinson, *Theory of Ordinary Differential Equations* (McGraw-Hill, New York, 1955), Chap. 13.

[45] H. Daido, Onset of cooperative entrainment in limit-cycle oscillators with uniform all-to-all interactions: Bifurcation of the order function, Physica D **91**, 24 (1996).

[46] C. van Vreeswijk, Partial synchronization in populations of pulse-coupled oscillators, Phys. Rev. E **54**, 5522 (1996).

[47] D. Golomb, D. Hansel, B. Shraiman, and H. Sompolinsky, Clustering in globally coupled phase oscillators, Phys. Rev. A **45**, 3516 (1992).

[48] D. Hansel, G. Mato, and C. Meunier, Clustering and slow switching in globally coupled phase oscillators, Phys. Rev. E **48**, 3470 (1993).

[49] F. P. Kemeth, S. W. Haugland, and K. Krischer, Symmetries of Chimera States, Phys. Rev. Lett. **120**, 214101 (2018).

[50] P. Ashwin and J. W. Swift, The dynamics of weakly coupled identical oscillators, J. Nonlin. Sci. **2**, 69 (1992).

[51] P. Ashwin, O. Burylko, and Y. Maistrenko, Bifurcation to heteroclinic cycles and sensitivity in three and four coupled phase oscillators, Physica D **237**, 454 (2008).

[52] Y. Kuramoto, Phase- and center-manifold reductions for large populations of coupled oscillators with application to non-locally coupled systems, Int. J. Bifurc. Chaos **07**, 789 (1997).

[53] A. Pikovsky and P. Rosenau, Phase compactons, Physica D **218**, 56 (2006).

[54] H. Kori, Y. Kuramoto, S. Jain, I. Z. Kiss, and J. L. Hudson, Clustering in globally coupled oscillators near a Hopf bifurcation: Theory and experiments, Phys. Rev. E **89**, 062906 (2014).

[55] C. Bick, M. J. Panaggio, and E. A. Martens, Chaos in Kuramoto oscillator networks, Chaos **28**, 071102 (2018).

[56] D. Pazó and E. Montbrió, From Quasiperiodic Partial Synchronization to Collective Chaos in Populations of Inhibitory Neurons with Delay, Phys. Rev. Lett. **116**, 238101 (2016); F. Devalle, E. Montbrió, and D. Pazó, Dynamics of a large system of spiking neurons with synaptic delay, Phys. Rev. E **98**, 042214 (2018).

[57] Otherwise, the frequency of (N)UIS would depend nonlinearly on ϵ, in disagreement with the MF-CGLE.

[58] C. Bick, M. Timme, D. Paulikat, D. Rathlev, and P. Ashwin, Chaos in Symmetric Phase Oscillator Networks, Phys. Rev. Lett. **107**, 244101 (2011).

[59] C. Bick, P. Ashwin, and A. Rodrigues, Chaos in generically coupled phase oscillator networks with nonpairwise interactions, Chaos **26**, 094814 (2016).

[60] P. Clusella, A. Politi, and M. Rosenblum, A minimal model of self-consistent partial synchrony, New J. Phys. **18**, 093037 (2016).

[61] C. Bick, Heteroclinic switching between chimeras, Phys. Rev. E **97**, 050201(R) (2018).

[62] P. S. Skardal and A. Arenas, Abrupt Desynchronization and Extensive Multistability in Globally Coupled Oscillator Simplices, Phys. Rev. Lett. **122**, 248301 (2019).

[63] M. Rosenblum and A. Pikovsky, Numerical phase reduction beyond the first order approximation, Chaos **29**, 011105 (2019).

[64] H. Kori and Y. Kuramoto, Slow switching in globally coupled oscillators: robustness and occurrence through delayed coupling, Phys. Rev. E **63**, 046214 (2001).